PHILOSOPHICAL TRANSACTIONS OF THE ROYAL SOCIETY A MATHEMATICAL, PHYSICAL & ENGINEERING SCIENCES

Palaeostress Determinations from Fault Kinematics: Application to the Neotectonics of the Himalayas-Tibet and the Central Andes [and Discussion]

J. L. Mercier, E. Carey-Gailhardis, M. Sebrier, S. Stein, J. L. Mercier, P. Hancock and P. England

Phil. Trans. R. Soc. Lond. A 1991 **337**, 41-52
doi: 10.1098/rsta.1991.0105

Palaeostress determinations from fault kinematics: application to the neotectonics of the Himalayas-Tibet and the Central Andes

By J. L. Mercier, E. Carey-Gailhardis and M. Sébrier

CNRS Laboratoire de Géophysique et Géodynamique Interne, Université Paris-Sud, Bât. 509, 91405 Orsay, France

This paper concerns the determination of the stress deviator from a set of striated faults or of focal mechanisms of earthquakes. Southern Tibet and the Cuzco region of the High Andes illustrate the applied methodology. Then, the spatial and temporal changes in the tectonic régimes of Tibet and Central Andes are briefly examined. The Quaternary–Present-day stress patterns in these two high plateaus favour models explaining the spatial changes in the state of stress at a large wavelength as a result of a compensated elevated topography. Major temporal changes in the tectonic régimes are attributed tentatively to uplift for the Tibetan plateau and, for the already elevated Andean Plateau, to changes in the magnitude of the boundary forces due to subduction processes.

1. Introduction

Knowledge of the spatial and temporal changes in the continental stress fields is of great importance in understanding the sources of what is called the 'tectonic stresses' (Zoback *et al.* 1989). Geological data contribute to the definition of the Recent and Present-day stress fields but in particular they permit one to demonstrate temporal changes in the state of stress over geological periods. Indeed, structural analyses concern deformations and therefore, to have access to stresses, there must exist a simple linear relation between the strain tensor and the stress tensor. Therefore, these structural analyses essentially concern small brittle deformations and assume the following hypotheses: (1) the analysed body of rock is physically homogeneous and isotropic and, if pre-fractured, is also mechanically isotropic, i.e. the orientation of the fracture planes is random; (2) displacements on the fault planes are small with respect to the fault lengths and there is no ductile deformation of the material, and thus no rotation of the fracture planes. In general, rocks are neither homogeneous nor isotropic but at the scale of bodies of rock, some tens of metres to some kilometres long, these assumptions are often valid and coherent results, obtained from numerous sites in a given region, often give a good approximation of the regional state of stress.

Habitually, fault orientations have been compared with the orientations of shear planes formed in a homogeneous and isotropic medium and have been related to the principal stress directions acting in this medium (Anderson 1951). But, because of the frequent occurrence of inherited fractures, the practical use of this method is very

Phil. Trans. R. Soc. Lond. A (1991) **337**, 41–52
Printed in Great Britain

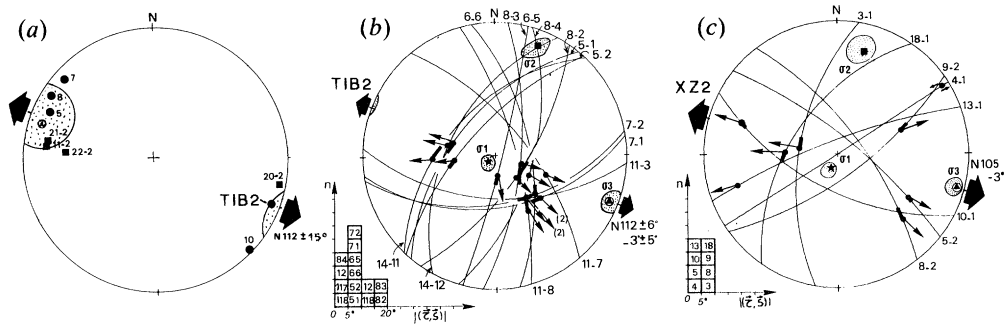

Figure 1. Quaternary and Present-day tensional (σ_3) directions in Tibet (figure 2) deduced from (*a*) recent minor normal faults. It shows Bingham statistics of the σ_3 axes obtained at different sites (Mercier *et al.* 1987), (*b*) major normal faults bordering the Yangbajin graben (TIB2), (*c*) focal mechanisms of teleseismic earthquakes (Carey-Gailhardis & Mercier 1987). Wulff stereonet, lower hemisphere, histograms give the deviations between the observed ($\boldsymbol{S}$) and predicted ($\boldsymbol{\tau}$) striations.

limited. Wallace (1951) and Bott (1959) have demonstrated that, if a pre-existing fault is reactivated, the orientation of the free slip on the fault plane depends on four parameters defining the principal stress reference and the stress ratio, $R = (\sigma_z - \sigma_x)/(\sigma_y - \sigma_x)$.

2. Palaeostress determination from fault kinematics in a fractured body of rock

(*a*) *Kinematics of faults measured in the field*

Using the mechanical approach of Wallace (1951) and Bott (1959), Carey & Brunier (1974) and Carey (1976) have proposed a quantitative computer-aided method to interpret the kinematics of a population of faults in a highly fractured body of rock. Their mechanical model assumes that the material is homogeneous and isotropic and that the deformations are small (see above) and, moreover, that (1) a tectonic event is characterized by a single homogeneous stress tensor, (2) the slip (responsible for the striation) occurs on each fault plane in the direction and sense of the resolved shear stress acting on the fault and (3) the slips are independent of each other. Then, deformation results from relative displacements of rigid blocks in an assemblage of blocks.

This model implies that the angle between the predicted $\boldsymbol{\tau}_i$ and the observed $\boldsymbol{S}_i$ slip-vectors is zero. The $\boldsymbol{\tau}_i$ components are a function of four parameters: the three Euler angles, which give the azimuthal directions of the orthogonal principal stress axes with respect to a geographical reference, and the relative ratio R of the principal deviatoric stress differences such that

$$R = (\sigma'_2 - \sigma'_1)/(\sigma'_3 - \sigma'_1)$$

(see demonstration in Carey (1976), and Carey-Gailhardis & Mercier (1987)). Numerous algorithms are now available to solve this problem. More sophisticated calculations are used to separate data corresponding to several states of stress. The reliability of the solutions obtained may be tested by calculation either of the deviations ($\boldsymbol{\tau}_i$, $\boldsymbol{S}_i$) on each fault plane or of the uncertainties in the principal stress directions (figure 1) and the R values.

PHILOSOPHICAL TRANSACTIONS OF THE ROYAL SOCIETY A MATHEMATICAL, PHYSICAL & ENGINEERING SCIENCES

(*b*) *Kinematics of faults deduced from focal mechanisms of teleseismic earthquakes*

The above numerical methods may also be applied to a population of focal mechanisms of teleseismic earthquakes, which have occurred in the same area, assuming a mean state of stress in the source region. This requires selection of the preferred seismic fault plane from each couple of nodal planes. This selection is made possible due to the fact that only one of the two slip vectors is the seismic slip in agreement with the principal stress axes. For this slip vector the R ratio, computed from Bott's (1959) formula, is such that $0 < R < 1$. Moreover, if one of the two nodal planes satisfies this condition, the other does not, except if the two nodal planes intersect each other along a principal stress axis (see Carey-Gailhardis & Mercier 1987). Generally, a population of focal mechanisms of major seismic events leads to a good evaluation of the regional state of stress in agreement with the state of stress deduced from Recent and active faulting (compare figure 1*a*, *b* and *c*).

(*c*) *Kinematics of faults deduced from focal mechanisms of aftershock sequences or of microseismic activity*

Focal mechanisms of aftershock sequences often show complex fault kinematics which result from heterogeneous deformation. Numerical analyses of such focal-mechanism data from regions submitted to an extensional tectonic régime (Mercier & Carey-Gailhardis 1989) clearly show a main group whose normal fault motions result from a tensional mean state of stress (TM) in good agreement with the regional state of stress deduced from recent Quaternary and active tectonics. The remaining complex fault motions are explained by compressional (TC) and/or tensional (TE) deviators. An important observation is that, within the uncertainties, these (TM), (TC) and (TE) deviators are coaxial. We suggest that in a highly fractured body of rock submitted to a state of stress, slip on many 'well-orientated' minor faults occurs so that motions of blocks statistically produced a deformation of the assemblage of blocks corresponding to the mean state of stress (TM). However, incompatibilities of block motions exist which induce internal elastic stresses in the blocks. These must be relaxed by slips on the block boundaries or by formation of new fractures. As these block displacements are constrained by the neighbouring blocks, it seems reasonable that these fault motions must be statistically compatible with the deformation of the whole assemblage and, thus, must be modelled statistically by deviators (TE, TC) having the same principal stress directions as those of the mean deviator (TM) but different values. Thus, provided some supplementary information about the active tectonic régime is known from other data, the (TM) deviator may be easily recognized. The (TE) and (TC) deviators model local slips and cannot be considered as other mean states of stress.

Detailed references concerning the numerical methods of stress determination from fault kinematics and earthquake focal mechanisms may be found in Zoback (1991), Zoback *et al.* (1989), Carey-Gailhardis & Mercier (1987) and Mercier & Carey-Gailhardis (1990).

(*d*) *Heterogeneous and homogeneous deformation of assemblages of rock blocks*

Thus data from the focal mechanisms of small earthquakes show that, in general, deformation of an assemblage of small blocks must be heterogeneous and that, in such a medium, motions of minor faults cannot be modelled by a single homogeneous stress deviator. However, it is a common observation that a population of striated

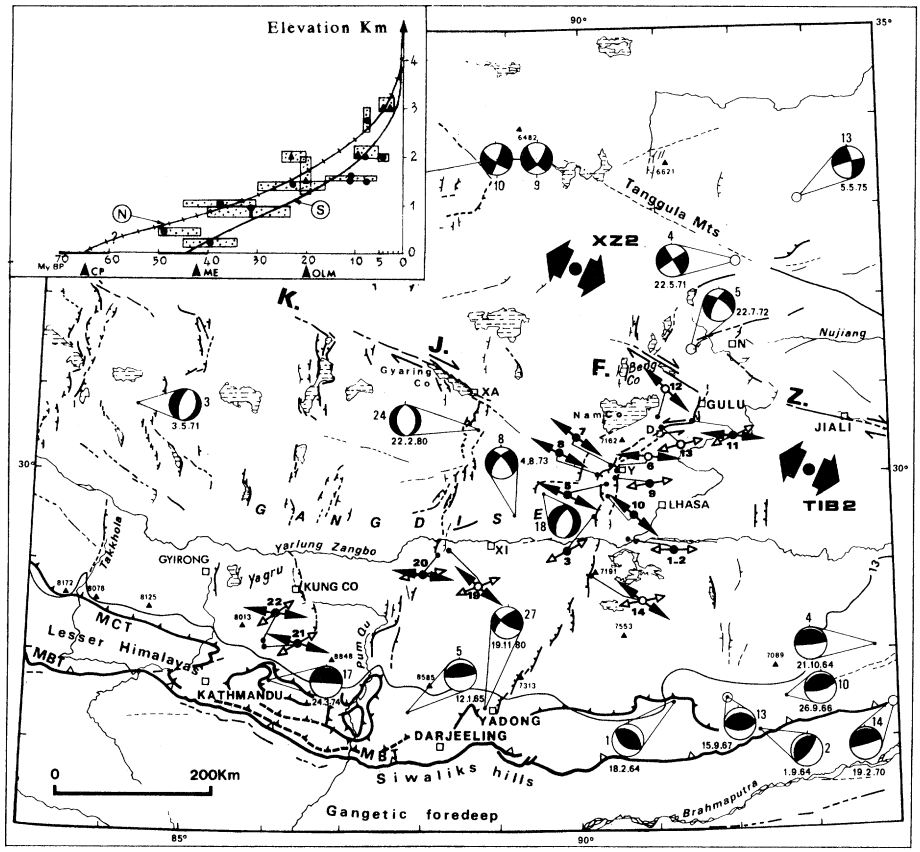

Figure 2. Seismotectonic map of Tibet (Mercier *et al.* 1987) showing the tensional directions deduced from analysis of recent minor faults (thin black arrows, figure 1*a*), major faults (large black arrows, TIB2, figure 1*b*) and focal mechanisms of teleseismic earthquakes (large black arrows, XZ2, figure 1*c*). Quaternary grabens are closely hachured. The inset (top left) schematically shows the Tibetan uplift inferred from variations of the vegetation in the Northern (N) and Southern (S) provinces.

faults, resulting from a single tectonic event, leads to the computation of a single stress deviator and this may appear surprising. It is noteworthy that numerous striations measured on faults in the field are mineral fibres and stylolitic striations which form by creep. In such a case, a pressure-dissolution process is active and annihilates the incompatibilities of block motions which should have existed as a result of stick–slip displacements.

3. Changes in the state of stress in Tibet during the Cenozoic and uplift of the high plateau

(*a*) *Analysis of fault kinematics in the field*

In Tibet geological mapping, satellite images and field observations (see references in Tapponnier *et al.* 1981 and Mercier *et al.* 1987) show that compressional structures striking E–W are cross-cut by N–S striking rift systems. Thus change in the tectonic régime is easily demonstrated. In the central part of the Indus–Zangbo suture,

reverse faults and backthrusts affect Oligo-Miocene (*ca.* 30–15 Ma) conglomerates. Their kinematics are in agreement with a N–S to NNE–SSW direction of shortening (Mercier *et al.* 1987). The rift systems have been active probably since the Pliocene (*ca.* 5 Ma). Motions of the recent minor normal faults, some tens to several hundreds metres long, are in agreement with tensional σ_3 axes (figure 2) whose mean direction trends $112° \pm 15°$ (figure 1*a*). The major faults, several kilometres long, which border the Yangbajin graben (figure 2) also show kinematics which agree with a σ_3 axis trending $112° \pm 6°$ (figure 1b). Finally, inversion of the focal mechanisms of teleseismic earthquakes located in a large area (figure 1*c*) shows that these are in agreement with a tensional σ_3 axis trending $105° \pm 7°$.

(*b*) *The spatial change in the present-day state of stress of the Himalayas-Tibet*

Thus the Tibetan plateau (mean altitude *ca.* 5000 m) is subjected to a tensional (σ_3) axis trending $112° \pm 6°$. On the other hand the Himalayan lowlands (altitude 300–1350 m above sea level) are subjected to a NNE–SSW trending compression (σ_1) as demonstrated by superficial folds and thrusts affecting Plio-Pleistocene deposits and by focal mechanisms of earthquakes (figure 2). Therefore, the maximum horizontal stress ($\sigma_{H,\,max}$) trajectory trends NNE–SSW, $022° \pm 6°$ in the high plateau, i..e roughly parallel to the India–Eurasia convergence in that central part of the India–Asia collision zone; $\sigma_{H,\,max}$ is σ_1 in the lowlands and σ_2 in the highlands. This spatial change in the state of stress favours models that explain the occurrence of normal faulting in Tibet as a consequence of its high elevation (Tapponnier & Molnar 1976; England & McKenzie 1982). These model emphasize the importance of topographic features of large extent which are compensated at depth by mass deficiencies due to a thick crustal root and a light asthenospheric mantle below it which perturb the vertical lithospheric stress σ_{zz} (see Fleitout & Froidevaux 1982). In the Himalayan lowlands, tectonics are compressional, thus $\sigma_{H,\,max}$ is σ_1 and σ_{zz} is σ_3. In regions of high elevation σ_{zz} increases with the topography. In the Tibetan plateau σ_{zz} exceeds $\sigma_{H,\,max}$, thus σ_{zz} is σ_1, $\sigma_{H,\,max}$ becomes σ_2 and $\sigma_{H,\,min}$ trending WNW–ESE becomes σ_3 thereby allowing extension to occur in this direction, i.e. orthogonal to the compressional direction acting in the adjacent lowlands (figure 2).

(*c*) *Temporal changes in the Cenozoic state of stress and uplift of Tibet*

Timing of the Tibetan uplift is supported by geological data provided essentially by palynological assemblages and coal beds (figure 2). These floral assemblages depend on the elevation above sea level but during the Pliocene–Quaternary overall climatic cooling has increased the effect of uplift on the floral environment. In spite of these uncertainties, it clearly appears that compressional structures of Upper Cretaceous–Palaeocene to Oligo-Miocene age formed in Tibet when its elevation was below an altitude of 2000 m. On the other hand, extension started during the Pliocene when the Tibetan plateau reached an elevation probably exceeding 3000 m. This observed temporal change in the state of stress gives additional support to the model that extension in the Tibetan plateau is a consequence of its high topography.

5. Changes in the state of stress in an already elevated plateau, the Andean plateau as an example

In the High Andes, the successive tectonic régimes during the Pliocene–Pleistocene are deduced from a detailed study of the successive fault kinematics. The Cuzco fault

PHILOSOPHICAL TRANSACTIONS OF THE ROYAL SOCIETY A MATHEMATICAL, PHYSICAL & ENGINEERING SCIENCES

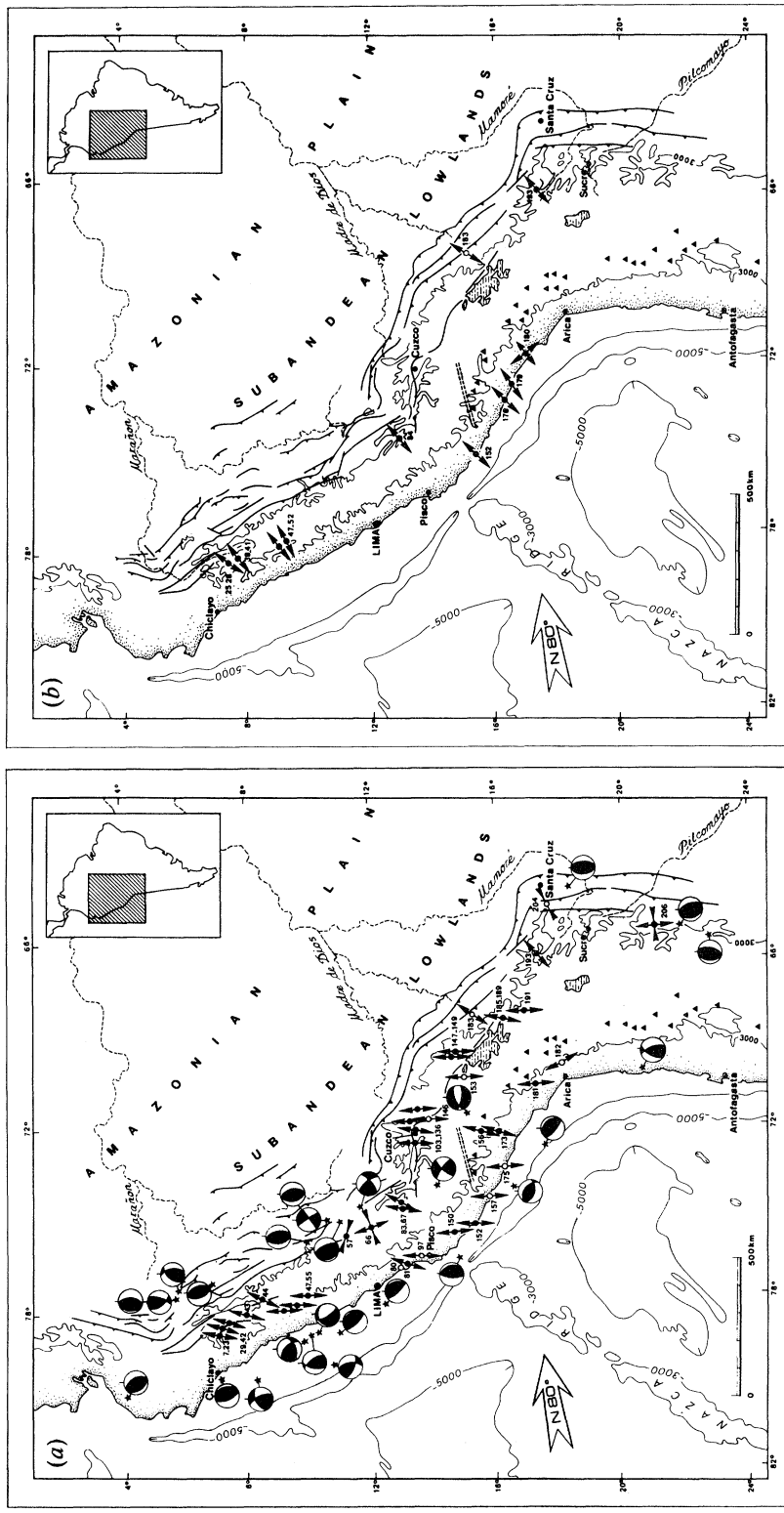

Figure 3. Principal stress directions deduced from analysis of fault kinematics in Peru and Bolivia. (*a*) Pleistocene and active faults and focal mechanisms of earthquakes, (*b*) NE–SW trending tensional σ_3 axes of latest Miocene–Pliocene age. Site numbers are those of Mercier *et al.*'s (1991) paper.

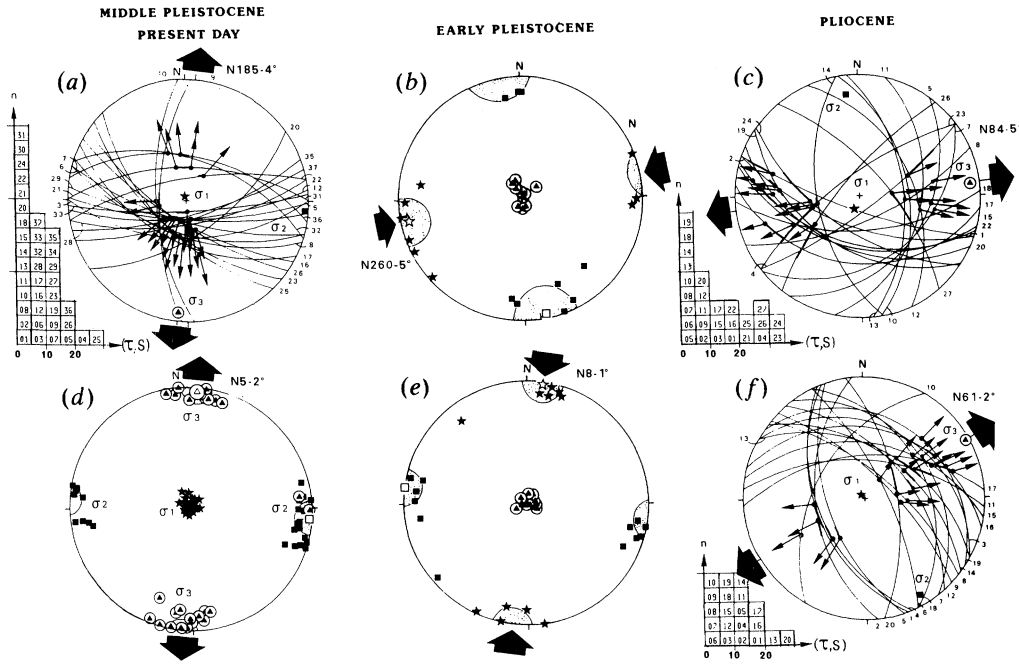

Figure 4. Fault slip-vector data and principal stress directions of the Cuzco region of (*a*), (*d*) Mid-Pleistocene to Present day, (*b*), (*e*) Early Pleistocene, (*c*), (*f*) and Pliocene age. Same symbols as on figure 1.

system (sites 103–109, figure 3*a*) in Peru is chosen as an example to illustrate the methodology used (see data in Sébrier *et al.* 1985, 1988; Mercier *et al.* 1991).

(*a*) *Analysis of fault kinematics in the field*

Minor faults have been analysed in the vicinity of the major fault system and in the adjacent grabens. Normal faults affecting Early Pleistocene (*ca.* 2–1 Ma) and Holocene (< 10 ka) deposits show kinematics which are in agreement with N–S trending tensional (σ_3) axes whose mean direction trends $005° \pm 6°$ (figure 4*d*). Compressional deformations also affect these Early Pleistocene deposits but they predate the deposition of terraces of Mid-Pleistocene age (*ca.* 0.4 Ma). They are synsedimentary and postsedimentary folds and reverse faults which are often offset by the above normal faults; normal striations superimposed upon reverse striations also are often observed on reverse fault planes. The kinematics of both synsedimentary and postsedimentary reverse faults are in agreement with either E–W or N–S compressional (σ_1) axes whose mean directions trend $260° \pm 10°$ and $008° \pm 7°$, respectively (figure 4*b*, *e*). An older normal faulting is coeval with sedimentation of lacustine and volcanic deposits. It postdates folding of probably latest Miocene age (*ca.* 7 Ma) and predates the above Early Pleistocene compression. This suggests that this older extension is of Pliocene age (*ca.* 5–2 Ma) which is clearly demonstrated in other regions of Peru. Kinematics of these synsedimentary faults are in agreement with tensional axes trending 060–090° (figure 4*f*).

The major fault planes affecting recent deposits, and observed in trenches dug across the seismic or Holocene fault 'scarplets', show a single direction of motion which is in agreement with a 185° trending σ_3 axis (figure 4*a*). However, the major

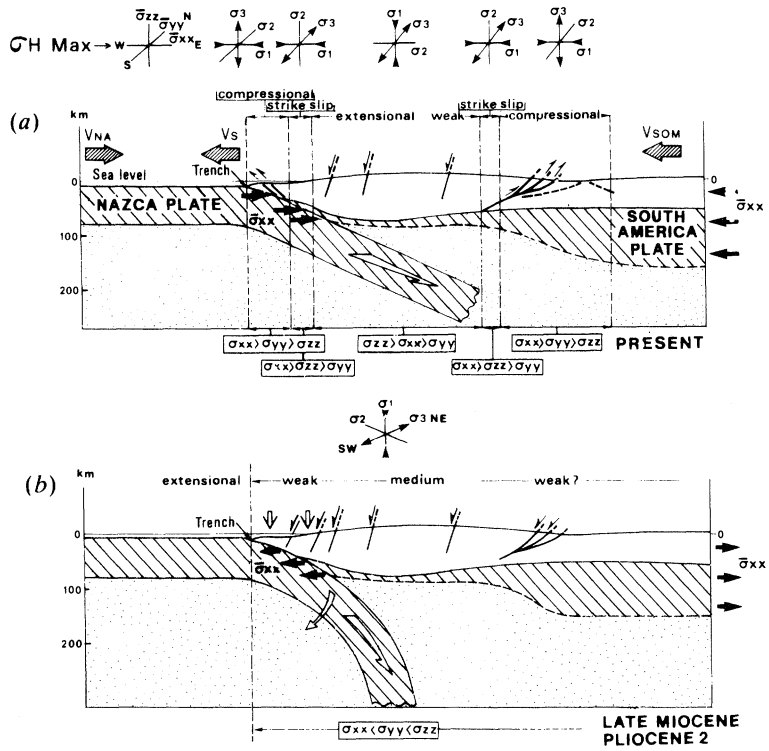

Figure 5. Suggested qualitative scenarios to interpret the change in the Andean state of stress (Mercier *et al.* 1991). (*a*) Present-day situation, σ_{xx} parallel to the convergence is $\sigma_{\mathrm{H,max}}$, N–S trending extension in the High Andes is an effect of compensated high topography (figure 3*a*); (*b*) Late Miocene–Pliocene situation, σ_{xx} is $\sigma_{\mathrm{H,min}}$ possibly as a result of slab retreat; a WNW–ESE extension is active, possibly throughout the whole Andes.

fault planes affecting the bed-rock show several superimposed families of striations. The younger striations are normal and agree with the above 185° trending tension. They postdate reverse and reverse strike–slip striations which belong to two different groups; one is in agreement with an E–W and the other with a N–S compression. The oldest striations are normal and are in agreement with a 085° trending σ_3 axis (figure 4*c*).

In conclusion, the successive kinematics of the major faults, when compared with the successive dated kinematics of the minor faults, permit one to establish a sequence of regional states of stress. In the High Andes this is as follows: (1) a Pliocene extensional tectonic régime having an NE–SW to E–W σ_3 axis, (2) an Early Pleistocene compressional tectonic régime showing two families of fault kinematics resulting from either an E–W or a N–S compression (σ_1) and (3) a Mid-Pleistocene–Present-day extensional régime having a roughly N–S σ_3 axis.

(*b*) *The spatial changes in the Present-day state of stress in the Central Andes*

A model of compensated elevated topography (figure 5*a*) is also convenient to explain the spatial change in the stress field in the Central Andes. A roughly E–W compression is active in the sub-Andean lowlands, along the Amazonian plain, and at the contact between the Nazca and South American plates and a roughly N–S extension is active in the High Andean plateau (figure 3*a*). Extensional tectonics

occurs at a mean elevation of *ca.* 3000 m, lower than in Tibet. This difference reflects the magnitudes of the compressive forces related to the convergence which are lower in the Andean subduction than in the Himalayan collision. In Peru, the tensional direction trends more NNE than expected from the 085° direction of convergence between the two plates.

(*c*) *The temporal changes in the state of stress in the High Andes during the Pliocene–Pleistocene*

The detailed analysis of temporal changes in the state of stress in the High Andes during this period is beyond the scope of this paper. Two important points must be emphasized: (1) the elevation of the Andes above sea level has not significantly changed during the past 5 Ma; (2) palaeomagnetic data show that the rotation of material in the Central Andes has been of the order of *ca.* 15° since the latest Miocene and cannot explain the differences between the σ_3 direction of Quaternary (figure 3*a*) and of Pliocene (figure 3*b*) age. Therefore, if the rheology of the Andean lithosphere has not changed significantly during this period, variations in magnitude of the boundary forces (figure 5*a*, *b*) are necessary to explain the changes in the tectonic régimes (figure 3*a*, *b*) during this period (see Mercier *et al.* 1991). These variations should be related to the subduction processes along the Andean margin (see, among others, Bott *et al.* 1989).

6. Concluding remarks

1. Many algorithms are now available to compute stress tensors from populations of faults or from earthquake focal mechanisms. The quality of the solutions obtained depends on the isotropy of the fault directions and on the deviations ($\boldsymbol{\tau}$, $\boldsymbol{S}$) between the observed ($\boldsymbol{S}$) and predicted ($\boldsymbol{\tau}$) slip vectors. Therefore, fault data should be reported on stereonets. These data must be clear enough to eventually permit digitization of the data. The histogram of the deviations ($\boldsymbol{\tau}$, $\boldsymbol{S}$) or the uncertainties in the stress directions (figure 1*b*, *c*) must be given also. In the database, this may be indicated by the mean and standard values of the deviations ($\boldsymbol{\tau}$, $\boldsymbol{S}$).

2. Concerning the palaeostress determination, as several deviators computed from a population of striated faults do not necessarily mean several actual states of stress (see §2*c*) it is of primary importance to indicate the geological data which have permitted one to separate the different tectonic régimes. Superimposed striations should be indicated on the stereographic projection of the faults with their relative chronology when observed. In the database the relative chronology of different families of striations at a given site, which lead to the computation of several stress tensors, should be indicated. The age of the formations affected by a family of striations and the age of the overlying formation, which is not affected by this family, should also be included in the database. Finally, it is useful to give the statistical mean direction of stress axes (σ_1 or σ_3 according to compressional or extensional régimes) obtained from minor fault sites and, if possible, to give the corresponding axis obtained from major faults in the same area (figure 4*a*, *d*).

3. Palaeostress determinations demonstrate temporal changes in the tectonic régimes and in the stress orientations which clearly show that the observed Present-day state of stress may not be extrapolated in general over long geological periods when formulating geodynamic reconstructions. The palaeostress-field analysis should be associated with palaeomagnetic studies to eventually demonstrate rotations of the stress directions 'frozen' in the material. Palaeostress fields are good indicators of

PHILOSOPHICAL TRANSACTIONS OF THE ROYAL SOCIETY A MATHEMATICAL, PHYSICAL & ENGINEERING SCIENCES

changes in the geodynamic conditions (see, among others, Philip 1987; Le Pichon *et al.* 1988; Zoback *et al.* 1991; Mercier *et al.* 1991).

This work has been supported by the programme DBT 'Instabilités' (contribution CNAS-INSU-DBT no. 351), Institut National des Sciences de l'Univers, Paris.

References

* Detailed references concerning the numerical methods of stress determinations are found in these references.

Anderson, E. M. 1951 *The dynamics of faulting*. Edinburgh: Oliver & Boyd.

Bott, M. H. P. 1959 The mechanics of oblique slip faulting. *Geol. Mag.* **96**, 109–117.

Bott, M. H. P., Waghorn, G. D. & Whittaker, A. 1989 Plate boundary forces at subduction zones and trench-arc compression. *Tectonophys.* **170**, 1–15.

Carey, E. 1976 Analyse numérique d'un modèle mécanique élémentaire appliqué à l'étude d'une population de failles: calcul d'un tenseur moyen des contraintes à partir des stries de glissement. *Thèse Univ. Paris-Sud, Orsay* (167 pages).

Carey, E. & Brunier, B. 1974 Analyse théorique et numérique d'un modèle mécanique élémentaire appliqué à l'étude d'une population de failles. *C.r. hebd. Séanc. Acad. Sci., Paris* **279**, 891–894.

*Carey-Gailhardis, E. & Mercier, J. L. 1987 A numerical method for determining the state of stress using focal mechanisms of earthquake populations. *Earth planet. Sci. Lett.* **82**, 165–179.

England, P. C. & McKenzie, D. P. 1982 A thin viscous sheet model for continental deformation. *Geophys. Jl R. astr. Soc.* **70**, 295–321.

Fleitout, L. & Froidevaux, C. 1982 Tectonics and topography for a lithosphere containing densities heterogeneities. *Tectonics* **1**, 21–56.

Le Pichon, X., Bergerat, F. & Roulet, M. J. 1988 Plate tectonics and tectonics leading to the Alpine belt formation, a new analysis. *Geol. Soc. Am.* **218**, 111–131.

Mercier, J. L., Armijo, R., Tapponnier, P., Carey-Gailhardis, E. & Han, T. L. 1987 Change from Late Tertiary compression to Quaternary extension in southern Tibet during the India–Asia collision. *Tectonics* **6**, 275–304.

*Mercier, J. L. & Carey-Gailhardis, E. 1989 Regional state of stress and characteristic fault kinematics instabilities shown by aftershock sequences: the aftershock sequences of the 1978 Thessaloniki (Greece) and 1980 Campania-Lucania (Italia) earthquakes as examples. *Earth planet. Sci. Lett.* **92**, 247–264.

Mercier, J. L., Sébrier, M., Lavenu, A., Cabrera, J., Bellier, O., Dumont, J. F. & Machare, J. 1991 Changes in the tectonic regime above a subduction zone of Andean Type: the Andes of Peru and Bolivia during the Pliocene-Pleistocene. *J. geophys. Res.* (In the press.)

Philip, H. 1987 Plio-Quaternary evolution of the stress field in Mediterranean zones of subduction and collision. *Annls Geophysicae* **87.03B**, 301–309.

Tapponnier, P. *et al.* 1981 The Tibetan side of the India–Eurasia collision. *Nature, Lond.* **294**, 405–410.

Tapponnier, P. & Molnar, P. 1976 Slip-line field theory and large-scale continental tectonics. *Nature, Lond.* **264**, 319–324.

Sébrier, M., Mercier, J. L., Mégard, F., Laubasher, G. & Carey-Gailhardis 1985 Quaternary normal and reverse faulting and the state of stress in Central Andes of South Peru. *Tectonics* **4**, 739–780.

Sébrier, M., Mercier, J. L., Machare, J., Bonnot, D., Cabrera, J. & Blanc, J. L. 1988 The state of stress in an overriding plate situated above a flat slab: the Andes of Central Peru. *Tectonics* **7**, 895–928.

Wallace, R. E. 1951 Geometry of shearing stress and relation to faulting. *J. Geol.* **59**, 118–130.

Zoback, M. L. 1991 First and second order patterns of stress in the lithosphere, World stress Map Project. *J. geophys. Res.* (In the press.)

*Zoback, M. L. *et al.* (29 authors) 1989 Global patterns of tectonic stresses. *Nature, Lond.* **341**, 291–298.

PHILOSOPHICAL TRANSACTIONS OF THE ROYAL SOCIETY A MATHEMATICAL, PHYSICAL & ENGINEERING SCIENCES

Discussion

S. Stein (*Northwestern University, Evanston, U.S.A.*). When the motion across the Peru–Chile Trench is examined from space geodetic data, that's the motion between Easter Island and Arequipa, about 15 mm a^{-1} of the motion that one would expect between the Nazca Plate and the central interior of South America is missing. What is happening?

J. L. Mercier. Indeed the motion between Easter Island and Arequipa shown by geodetic data appears to be anomalous and we have no certain explanation to propose. However, taking into account the fact that the sub-Andean shortening is about ten times higher along the Bolivian orocline (14–19° S) than further north, i.e. along the Huancabamba traverse (5° S), one might expect a slower convergence rate in the area of the Arica elbow (18° S).

P. Hancock (*Bristol University, U.K.*). Fault striation analysis is a very powerful and elegant technique, but there is just one assumption that I have never understood and that is that the striation on all faults will be parallel to the resolved shear stress. This is a reasonable assumption, if we assume that all the faults are independent elliptical surfaces, but if they interact, as we know many real fault systems do, with perhaps two or three faults interacting, the sense of slip will be partly determined by the shape of the block and won't always be parallel to that resolved shear stress.

J. L. Mercier. It is a real fact that in a highly fractured body of rock fault motions are not independent. Focal mechanisms of aftershock sequences and microseismic activity show that deformation of an assemblage of small blocks is heterogeneous and cannot be modelled by a single homogeneous stress deviator. This results from incompatibilities of motions of neighbouring blocks. Yet it is noteworthy that numerous fault striations measured in the field are mineral fibres and stylolitic striations which form by creep. In these cases a pressure-dissolution process has annihilated the incompatibilities of fault motions. I had no time to explain this during my talk; it concerns §§2*c* and *d* of our paper.

P. England (*Oxford University, U.K.*). If both horizontal principal stresses are tensional, why are there strike–slip faults in the Himalayas?

J. L. Mercier. Supposing that $\sigma_{\mathrm{H,\,max}}$, due to the convergence, and σ_{zz} remain constant, the deviatoric σ_2 value in the high plateau depends on the E–W boundary forces. Because the southern part of the plateau, between the Himalayan syntaxes (see Mercier *et al.* 1987, fig. 12), does not have the possibility to 'flow' in the E–W direction, the deviatoric σ_2 value must be weakly compressional or extensional (stress ratio $R \geqslant 0.45$). Because the northern part of the plateau does have the possibility to extend in an E–W direction, the deviatoric σ_2 value must be compressional ($R < 0.5$). Numerical simulations show that if the σ_2 value is extensional, only nearly vertical faults (except those normal to σ_3) may have a strike–slip motion; other faults, whatever their strikes, have high normal components of motion (see the stereonet in figure 1*b* of recent faults in Southern Tibet; $R = 0.46 \pm 0.14$). If the σ_2 deviatoric value is compressional, faults having dips less than 70° may have a strike–slip motion, especially those striking 060–070° and 150–160°

(see stereonet in figure 1*c* of seismic faults from focal mechanisms of Northern Tibet earthquakes, $R = 0.17 \pm 0.07$). Differences in fault motions are seen in these two cases when one compares the motions of the faults labelled 11-7 (figure 1*b*) and 8-2 (figure 1*c*) which have roughly the same strike and dip (this problem has been discussed in Mercier *et al.* (1987), §4.3, fig. 12).